Switchable Polarization Rotation of Visible Light Using a Plasmonic Metasurface

Stuart K. Earl, [1,a)] Timothy D. James,[1] Daniel E. Gómez,[2,3] Robert E. Marvel,[4,5] Richard F. Haglund Jr.[5] and Ann Roberts[1]

[1]*School of Physics, The University of Melbourne, Victoria, Melbourne, 3010, Australia*

[2]*CSIRO Manufacturing Flagship, Private Bag 33, Clayton, Victoria, 3168, Australia*

[3]*The Melbourne Centre for Nanofabrication (MCN), Australian National Fabrication Facility, Clayton, Victoria, 3168, Australia*

[4]*Interdisciplinary Materials Science Program, Vanderbilt University, Nashville, Tennessee 37235, USA*

[5]*Department of Physics and Astronomy, Vanderbilt University, Nashville, Tennessee 37325, USA*

[a)] Electronic mail: s.earl@student.unimelb.edu.au

A metasurface comprising an array of silver nanorods supported by a thin film of the phase change material vanadium dioxide is used to rotate the primary polarization axis of visible light at a pre-determined wavelength. The dimensions of the rods were selected such that, across the two phases of vanadium dioxide, the two lateral localized plasmon resonances (in the plane of the metasurface) occur at the same wavelength. Illumination with linearly-polarized light at 45 degrees to the principal axes of the rod metasurface enables excitation of both of these resonances. Modulating the phase of the underlying substrate, we show that it is possible to reversibly switch which axis of the metasurface is resonant at the operating wavelength. Analysis of the resulting Stokes parameters indicates that the orientation of the principal linear polarization axis of the reflected signal is rotated by 90 degrees around these wavelengths. Dynamic metasurfaces such as these have the potential to form the basis of an ultra-compact, low-energy multiplexer or router for an optical signal.

I. Introduction

Plasmonic metasurfaces that display dynamically modulated resonances have been demonstrated over a range of frequencies from the THz[1] to the visible.[2] This can be achieved by altering the material properties of the resonant metal, manipulating the dielectric environment, elastic/inelastic deformation of the device or varying the method of illumination. Plasmonic modulation has already been demonstrated using a variety of these methods, such as photoexcitation of free carriers,[1] mechanical deformation,[3, 4] incorporation within a matrix of a liquid crystal,[5] and phase change materials.[2, 6-10] The development of devices facilitated by these dynamic, reversibly-tunable structures is one of the next steps in the translation of plasmonic structures into functional devices.

The localized surface plasmon (LSP) resonance of a subwavelength metallic structure is directly related to the composition and properties of its constituent materials, dielectric environment and geometry.[11, 12] For example, a red-shifting of the plasmon modes of a silver nanocube on an ITO-glass substrate was observed with increasing refractive index of the superstrate.[13]

A rod on a substrate displays two LSP modes with their dipole moments parallel to the substrate, each aligned to the one of the two axes of the rod, as well as a third whose dipole moment extends out of the plane of the substrate.[14] By varying the angle of incidence and polarization state of the incident light a superposition of these different modes can be excited.[15] In the presence of a substrate, the resulting asymmetry in the dielectric environment of the rod leads to a strong separation in resonance frequency between the in-plane and out-of-plane LSP modes. The frequencies at which these modes occur are dependent on the value of the dielectric permittivity of the substrate/superstrate and the dimensions of the rod.[16] Thus, altering the optical properties of the substrate modifies the frequencies of the LSP resonances of the rod. This effect is the mechanism by which phase-change materials such as vanadium dioxide (VO_2) modulate plasmon resonances.

VO_2 is considered an insulator at room temperature, but, if heated to temperatures higher than 68°C, it becomes conductive,[17] its crystalline structure transitions from monoclinic to rutile[18, 19] and the real part of its refractive index decreases. This phase is commonly referred to as the metallic phase. The phase transition can be triggered not only thermally, but also by application of mechanical stress,[20] applied current/voltage[21, 22] or optically.[23] Significantly, when triggered optically by femtosecond laser pulses, VO_2 has been shown to transition on a sub-picosecond timescale, indicating potential for ultrafast plasmonic modulation devices.[24-28] The insulator-to-metal transition (IMT) is percolative,[29, 30] while the metal-to-insulator transition (MIT) process appears completely random. This process of individual crystal grains undergoing a transition leads to both phases occurring simultaneously in the same film,[31] enabling access to a range of intermediate effective material properties between the two extremes represented by the insulating and metallic phases. VO_2 has previously been used to modulate the extinction of a plasmonic waveguide[32] and nano-gap junctions,[33] as well as the spontaneous emission from a layer of quantum emitters via its manipulation of the local density of optical states.[34]

Here we fabricated an array of silver nanorods on a thin film of VO_2, and harness the dielectric shift caused by the VO_2 phase-change to manipulate the resulting polarization axis of a reflected signal at a specified wavelength. Our results show that at the central operating wavelength of the metasurface, the principal polarization axis of the reflected light is rotated by 90° when the phase of the underlying substrate is modulated. This is facilitated by the change in the real part (n) of the refractive index of VO_2 when transitioned from the insulating (ambient temperature) phase to its metallic (>68°C) phase. Figure 1(a) presents a schematic showing this far-field behavior, highlighting how it is possible to rotate the principal polarization axis by modulating the phase of the substrate.

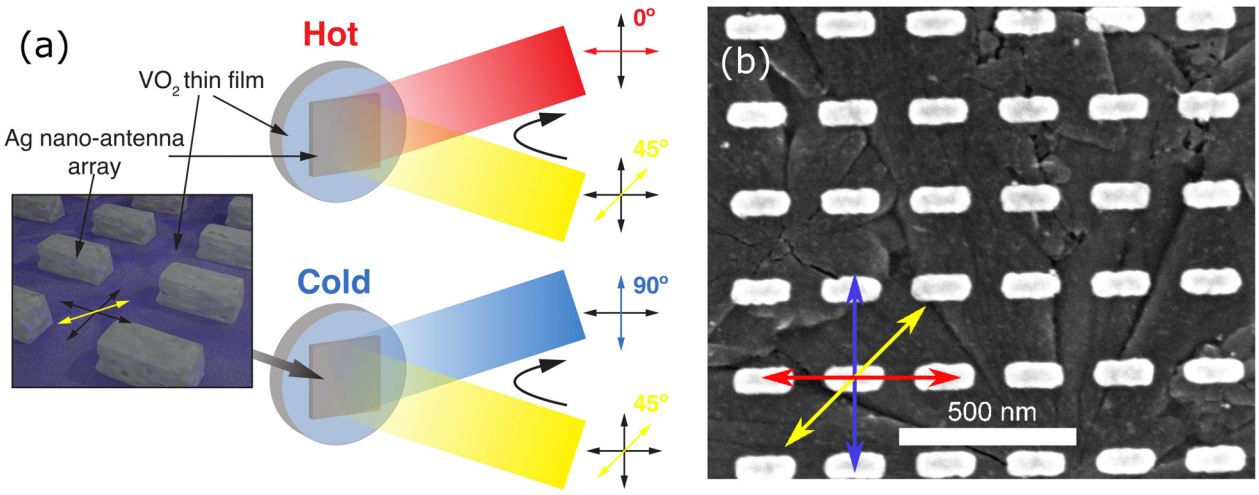

Figure 1: (a) Visualization of the operation of the polarization switch. Incident linear polarized light at 45° to the rod axes excites the lateral LSP resonances of the array. At the design wavelength the principal polarization axis of the reflected light is parallel to the electric dipole moment of the LSP, whose orientation is dependent on the phase of the underlying VO_2; (inset) schematic representation of the various polarization axes of interest during experiments; yellow shows the orientation of the polarization axis of the incident light while the blue/red arrows indicate the resonant axis at the wavelength of interest on insulating/metallic VO_2 respectively. (b) SEM of the fabricated nanorod array; the background texture is the structuring of the underlying VO_2.

II. Metasurface Design

A nanorod on a substrate of the insulating phase of VO_2 will display LSP resonances that are red-shifted relative to an identical rod on VO_2 in its metallic phase. This substrate-dependent dielectric shift therefore permits the dimensions of the short axis of a nanorod on a substrate of insulating VO_2 and those of the long axis on metallic VO_2 to be chosen such that the orthogonal LSP resonances are spectrally aligned.

This overlap of perpendicular LSP modes enables manipulation of the principal polarization axis of the reflected light via modulation of the substrate phase. It is well known that the orientation of the resonant axis of a rod supporting an LSP induces a polarization orientation in the reflected signal parallel to its electric dipole moment. Changing the VO_2 phase will therefore rotate the primary axis of the reflected signal by 90^0, creating a reversible, compact and easily-integrated method of changing the orientation of the polarization axis in a thin film device.

Design and Simulation

To design the plasmonic metasurface, we found numerical solutions to Maxwell's equations via the finite element method (FEM) implemented in the RF module of COMSOL Multiphysics.[35] A square array of periodicity 250 nm of Ag nanorods on a silicon substrate supporting a thin film of VO_2 was simulated. The height of the modelled domain was 1.5 µm. Excitation was provided by a port boundary condition on the upper half-space (n=1, air side), and periodic boundary conditions were used on the transverse boundaries. Since only normal incidence excitation was used, and since only the zeroth-order

reflection was present in the wavelength range of interest, the port boundary was sufficient to terminate any reflections. The lower boundary (in the substrate) was simulated via a scattering boundary to absorb any transmitted signal, preventing any reflections from this lower surface. The optical properties of silicon and silver were taken from Palik,[36] while the optical constants of VO_2 were taken from Earl *et al*.[2] A parametric sweep was performed to ascertain a relationship between rod length, VO_2 phase and plasmon resonance wavelength. As we have shown previously,[37] the thickness of the underlying VO_2 also affects the peak plasmon resonance wavelength, and so its thickness was set to a constant value of 110 nm to maximize the amplitude of the reflected signal around the wavelength range of interest. The outcome of these simulations, shown in figure 2(a), found that a square-periodic array of 50 nm (140 nm) long nanorods on insulating (metallic) VO_2 supports an LSP centered on 750 nm.

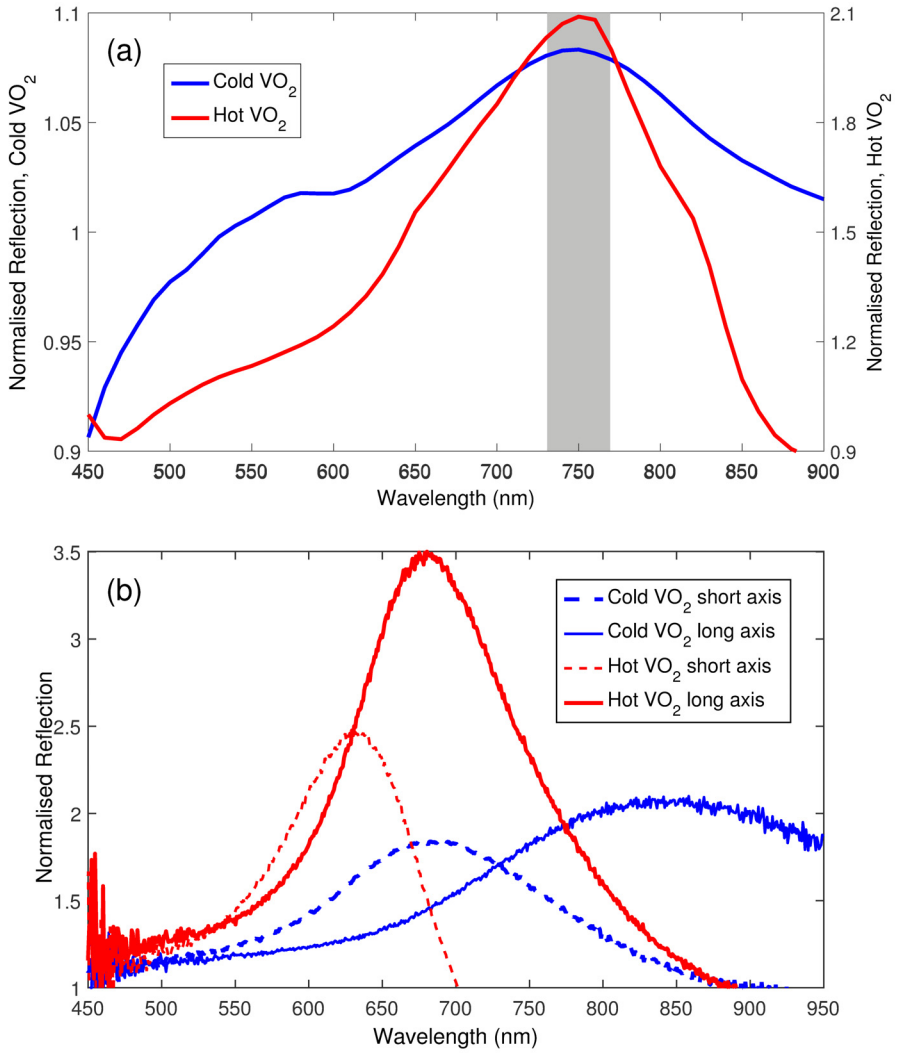

Figure 2 (a) FEM simulations of the normalised reflectance from a silver nanorod array on cold (hot) VO_2 50nm (140 nm) long, illuminated by normally-incident white light polarized parallel to the nanorod. The peaks overlap due to the different refractive indicies of the two phases of the underlying VO_2; (b) Normalised reflectance for an input polarizer angle of 45° for the analyzing polarizer both parallel to the long axis of the rods (solid lines) and orthogonal to them

(broken lines). The central operating wavelength of the device is at the overlap of the two orthogonal resonances, shown here at 685 nm.

III. Experimental Results

Electron beam lithography (EBL) was used to fabricate silver nanorod arrays on thin films of VO_2. Details of the deposition of the VO_2 thin films and subsequent EBL processes are given in the Supplementary Information. The surface structure of the VO_2 displayed a small level of porosity and an rms roughness of around 7 nm (measured using atomic force microscopy and incorporated into the ellipsometry fitting algorithm). Figure 1(b) shows an SEM of the metasurface, with color-coded arrows indicating the relevant polarization axes.

Normal incidence spectroscopy from the air side of the metasurface was performed as a function of both input and output angle of polarization. Supplementary figure S1 presents a schematic and details of the experimental setup. Reflectance spectroscopy was used due to the supporting Si substrate being opaque at the wavelengths of interest.

Figure 2(b) shows the normalised reflectance ($R_{norm} = R_{array}/R_{substrate}$) from the rod arrays for an input polarization of 45° and an analyzer (the second linear polarizer immediately preceding the spectrometer) orientation parallel to each of the rod axes in turn. The normally-incident, 45° linearly polarized light excites both the dipolar LSP modes that lie in the plane of the substrate and facilitates simpler analysis due to its known polarization state. From the large shift in the peak reflected wavelength (as the analyzer, initially parallel to the rods' long axis, is rotated 90°) it is clear that the reflected signal is significantly linearly polarized. For the complete set of measurements refer to the Supplementary Information, figure S2.

For insulating VO_2 ("Cold VO_2", T ~ 22°C) the rod array resonances are measured at 690 nm (short axis) and 841 nm (long axis). For metallic VO_2 ("Hot VO_2", T > 80°C) the rod arrays displayed resonances at 632 nm (short axis) and 679 nm (long axis). Hence, for 45° linearly polarized (or unpolarized) incident light near wavelengths of 680 nm the primary polarization axis of the reflected light can be rotated by 90° by switching the phase of the VO_2 substrate.

IV. Discussion

Experimental measurements displayed a blue-shift of around 50 nm from the design wavelength, and the optimum rod dimensions for the LSP resonances also deviated from that predicted by COMSOL. While there are a number of explanations for this, from inaccuracies in evaporated film thicknesses, the assumed optical properties of silver (bulk properties were used),[36] the native oxide present on the silver or inhomogeneities in rod dimensions, variations in the optical properties of the VO_2 film were thought to be the primary cause. VO_2 films are known to demonstrate a variation in optical properties

dependent on deposition method and stoichiometry.[37-39] Ellipsometry was performed on the specific VO_2 films used here and numerical simulations using those results were performed; results of both are presented in the Supplementary Information (figures S3 and S4). A high level of agreement between the experimental and numerical results is apparent, suggesting that the optical properties of each individual film is the primary cause of the noted disparity. Despite this blue-shift, the overlap of the orthogonal LSP modes centred on 680 nm, however, enables the device to perform as desired.

While analysis of the normalised reflectance facilitates understanding of the spectral location of the plasmon resonances, a realistic device requires significant modulation of the absolute magnitude of the reflected signal to operate. The absolute signal from our device is compared to that from the bare substrate in the Supplementary Information, figure S5. Analysis of the absolute signal permits identification of the operating range of the device. For these metasurfaces the maximum functional range spans from 641 nm to 734 nm, with a central operating wavelength of 679 nm.

V. Polarization analysis

Further insight into the polarization behavior of the metasurface can be obtained by characterizing the Stokes parameters of the reflected signal. The Stokes parameters (S_0, S_1, S_2 and S_3) give detailed information about the polarization state of electromagnetic radiation.[40,41] Specifically, the S_1 value represents the degree of linear polarization parallel to the rod axes (the Stokes parameters are discussed briefly in the Supplementary Information). In relation to these measurements, an S_1 value of +1 indicates 100% linearly polarized wave with its polarization oriented parallel to the short axis of the rods while a value of -1 indicates 100% linearly polarized with orthogonal polarization. It is worth highlighting here that the presented values, S_1, S_2 and S_3, are normalised to total intensity, S_0.

The Stokes parameters were measured using normally incident light that was linearly polarized at 45° to the primary nanorod axes in the manner of Collet *et al*.[41] The resulting intensity measurements are dependent on different polarized components within the incident beam and therefore permits calculation of the Stokes parameters.

Figure 3 shows the S_1 value as a function of wavelength for the rod array with an incident linear polarization (a) parallel, (b) at 45° and (c) orthogonal to the short axis of the rods. The relative orientation of the arrows inset in the figure highlight the implication of the sign of the S_1 parameter. Below 500 nm and above 850 nm the experimental data is unreliable due to the limited operating wavelength ranges of the polarizing elements, beam splitters and other optical elements. While figures 3(a) and (c) show little variation from the incident polarization state, figure 3(b) indicates that in the vicinity of the resonance wavelengths of the rod LSPs the metasurface has a significant influence upon the polarization state of the reflected light. The

complete set of Stokes parameters for input linearly polarized light at 0°, 45° and 90° relative to the short axis of the rods are presented in the Supplementary Information, figure S6.

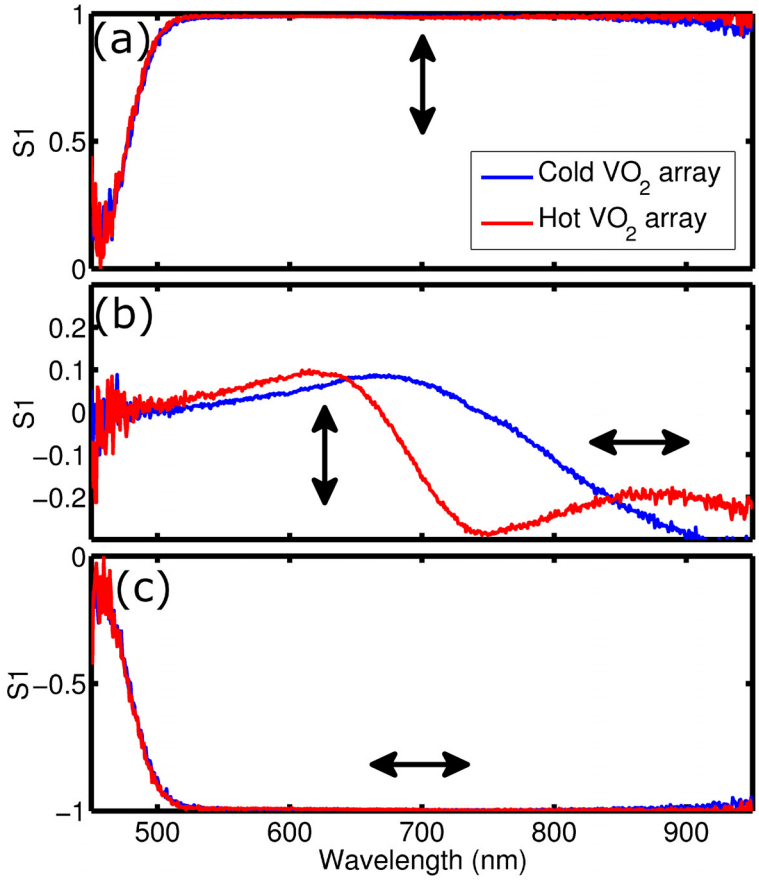

Figure 3: Stokes vector (S_1) as a function of wavelength for linearly polarized input white light at an angle of 45° to the rod axes. Solid lines show the S_1 vector of the array on insulating (blue) and metallic (red) VO_2 in reflection with the input linear polarizer orientated at (a) 0°, (b) 45° and (c) 90° to the rods' short axis. The arrows inset on the plots show how the sign of the S1 parameter relates to the orientation of the polarization axis of the reflected signal, with a positive S1 value indicating "vertical" polarized light and a negative value indicating a "horizontal" polarization.

For incident light polarized at 45° to the rod axes, in the vicinity of the short axis resonances (683 nm insulating and 630 nm metallic VO_2), S_1 increases to 0.1 before decreasing to -0.3 around the long axis resonances (850 nm insulating and 680 nm metallic VO_2). At the central operating wavelength of the array a total change in linear polarization can then be found by calculating the difference in these two values at that wavelength, which for 679 nm is a change of over 13%. Significantly, the sign of the S_1 vector changes at this wavelength, indicating that the reflected signal goes from being partially vertically polarized (parallel to the short axis of the rods) to partially horizontally polarized (parallel to the long axis of the rods). The largest difference between the two S_1 vectors occurs at 733 nm and is a much larger 29.6%. It is worth noting that at wavelengths longer than 750 nm there is a significant degradation in the response of the beam splitter (Thorlabs BS013),[39]

and so the data used to calculate the Stokes parameters at these wavelengths must be regarded as questionable. They do, however, demonstrate that the array is indeed affecting the polarization of the reflected light, confirming that the LSP resonances are the driving mechanism behind the changes in reflected polarization observed.

A useful metric for assessing the performance of the polarization-modulating metasurface is the percentage of the reflected intensity in the desired polarization state. The incident light can be considered completely polarized at 45^0 to the nanorod axes. Supplementary figure S6(e) gives the S_2 parameter for the incident 45^0linearly polarized light. At wavelengths shorter than those of the LSP resonances of the nanorods, the S_2 parameter displays a value of +1, which indicates that 100% of the reflected light displays a +45° linear polarization state. Since the metasurface displays no resonance in this wavelength range (refer to supplementary figure S2) it will reflect the incident polarization state essentially unperturbed. Hence, we can assume that the incident light across the entire visible spectrum exhibits an identical polarization.

A silver mirror (Thorlabs PF10-03-P01) was used in place of the VO_2 substrate to characterize the source, thus permitting calculation of the amount of incident light transformed into the desired polarization state. This figure of merit represents the absolute efficiency of the metasurface. At the central operating wavelength of 679 nm, the bare VO_2 film in its insulating (metallic) phase reflected 27.7% (11.8%) of the incident light. The normalised reflectance of the silver nanorod arrays on the VO_2 was 1.532 (insulating) and 1.913 (metallic). The metasurface therefore reflected 42.4% and 22.6% of the incident signal in the insulating and metallic phases respectively.

The normalised Stokes parameters (S_1) at this wavelength were measured to be +0.08 (insulating) and -0.04 (metallic), which, translated in to a percentage of the incident signal, indicates that 3.4% and 0.9% of the incident light were directed into the desired linear polarization states. The remainder of the incident light was either absorbed by the opaque substrate, the VO_2 thin film and the nanorod array, or reflected into another polarization state.

The relatively low efficiency of this device can be improved in a number of ways. Here, we have focussed on a proof-of-concept device operating in the visible spectrum. The larger contrast between the optical phases of the enabling VO_2 in the near IR, however, suggests a superior device may be possible. An IR polarization rotating device is the subject of active research, although it represents a significantly different device to the one proposed here.

A challenge in the design of this device is the amplitude and width of the reflected signal from the two rod axes. Due to the lower absorption of silver at longer wavelengths, the two lateral resonances of the rods will always have different amplitudes. In addition, the higher absorption of the insulating phase of VO_2 will produce broader resonances compared to the metallic phase. There are several methods that could be used to ameliorate these issues. The incident polarization angle onto the array could be optimized to favor the weaker shorter-axis resonances, and the periodicity could be altered to increase the amplitude

of the reflected signal for that axis. For simplicity here we have elected to restrict the experiment to the simpler parameters above to focus on the mechanism behind the polarization response.

VI. Conclusion

We have presented a proof-of-concept design of a metasurface that uses the orthogonal LSP resonances of a nanorod array to modulate the linear polarization state of the light it reflects. This was achieved by selecting the appropriate dimensions of the nanorods such that the lateral LSP modes occurred at the same pre-determined wavelength across the VO_2 phase change. This mechanism is repeatable, and easily reversed by simply lowering the temperature of the substrate.

We measure a 13% change in the total linear polarization for the signal reflected from our device at its central wavelength, as well as a sign change of the Stokes S_1 parameter, indicating a change from predominantly horizontally to vertically linearly-polarized light. In conjunction with a linear polarizer to filter a specific linear polarization axis, we show this difference to be sufficient to clearly detect the change in signal. While the portion of incident light transformed to the desired polarization state is low, the signal switched between orthogonal states is sufficient to be detected, and hence, to form the basis of a useful device.

The operating wavelength of our device can be tuned by altering the dimensions of the metal nanorods in the array: increases in these dimensions could result in operating wavelengths in the infrared. This would increase the separation between the two lateral resonances of the rods, increasing the refractive index contrast across the VO_2 phases and therefore the effectiveness of the device. Devices such as this may therefore be of use in next generation optical circuits and other plasmonically-enabled devices.

Supplementary Information

Supporting Information contains details of the fabrication and characterization processes, normalised reflectance measurements for all combinations of input and analyzing polarizer angles at 0°, 45° and 90° polarizer to array rods axes, the results of spectroscopic ellipsometry of VO_2 and a comparison of numerical and experimental data. The absolute signal reflected from the sample is given. Also provided is a brief explanation of the Stokes parameters to give context for the discussion, and the full set of measured Stokes parameters for input linearly polarized light at 0°, 45° and 90° to the rod axes.

Acknowledgements

The authors would like to acknowledge the financial support of the Australian Research Council (project number FT140100514, DP110100221 and DP110101767), the Defence Science Institute, a Vanderbilt University/University of

Melbourne collaboration grant and a Melbourne Centre for Nanofabrication Technical Fellowship. This work was performed in part at the Melbourne Centre for Nanofabrication (MCN) in the Victorian Node of the Australian Fabrication Facility (ANFF). R. E. M. and R. F. H. acknowledge support of this work from the National Science Foundation (DMR-1207507) and from Vanderbilt University, office of the Vice Provost for Research.

References

1. Padilla, W.; Taylor, A.; Highstrete, C.; Lee, M.; Averitt, R., Dynamical electric and magnetic metamaterial response at terahertz frequencies. *Phys. Rev. Lett* **2006***, 96 (10),* 107401.

2. Earl, S. K.; James, T. D.; Davis, T. J.; McCallum, J.; Marvel, R.; Haglund, R. F.; Roberts, A., Tunable optical antennas enabled by the phase transition in vanadium dioxide. *Opt. express* **2013***, 21 (22),* 27503-27508.

3. Ou, J.; Plum, E.; Jiang, L.; Zheludev, N., Reconfigurable photonic metamaterials. *Nano lett.* **2011***, 11 (5),* 2142-2144.

4. Huang, F.; Baumberg, J., Actively tuned plasmons on elastomerically driven Au nanoparticle dimers. *Nano. lett.* **2010***, 10 (5),* 1787-1792.

5. Kossyrev, P.; Yin, A.; Cloutier, S.; Cardimona, D.; Huang, D.; Alsing, P.; Xu, J., Electric field tuning of plasmonic response of nanodot array in liquid crystal matrix. *Nano lett.* **2005***, 5 (10),* 1978-1981.

6. Jeong, Y.-G.; Bernien, H.; Kyoung, J.-S.; Park, H.-R.; Kim, H.-S.; Choi, J.-W.; Kim, B.-J.; Kim, H.-T.; Ahn, K.; Kim, D.-S., Electrical control of terahertz nano antennas on VO_2 thin film. *Opt. express* **2011***, 19 (22),* 21211-21215.

7. Suh, J. Y.; Donev, E. U.; Ferrara, D. W.; Tetz, K. A.; Feldman, L. C.; R. F. Haglund, J., Modulation of the gold particle–plasmon resonance by the metal–semiconductor transition of vanadium dioxide. *J. Opt. A-Pure Appl. Op.* **2008***, 10,* 4169-4175.

8. Kaplan, G.; Aydin, K.; Scheuer, J., Dynamically controlled plasmonic nano-antenna phased array utilizing vanadium dioxide. *Opt. Mater. Express* **2015***, 5 (11),* 2513-2524.

9. Dicken, M. J.; Aydin, K.; Pryce, I. M.; Sweatlock, L. A.; Boyd, E. M.; Walavalkar, S.; Ma, J.; Atwater, H. A., Frequency tunable near-infrared metamaterials based on VO_2 phase transition. *Opt. express* **2009***, 17 (20),* 18330-18339.

10. Markov, P.; Appavoo, K.; Haglund, R. F.; Weiss, S. M., Hybrid Si-VO_2-Au optical modulator based on near-field plasmonic coupling. *Opt. express* **2015***, 23 (5),* 6878-6887.

11. Maier, S. A.; Atwater, H. A., Plasmonics: Localization and guiding of electromagnetic energy in metal/dielectric structures. *J Appl Phys* **2005,** *98 (1)*, 011101.

12. Willets, K. A.; Van Duyne, R. P., Localized surface plasmon resonance spectroscopy and sensing. *Annu. Rev. Phys. Chem.* **2007***, 58,* 267-297.

13. Mahmoud, M. A.; Chamanzar, M.; Adibi, A.; El-Sayed, M. A., Effect of the dielectric constant of the surrounding medium and the substrate on the surface plasmon resonance spectrum and sensitivity factors of highly symmetric systems: silver nanocubes. *J. Am. Chem. Soc.* **2012***, 134 (14),* 6434-42.

14. Auguié, B.; Barnes, W. L., Collective resonances in gold nanoparticle arrays. P*hys. Rev. Lett.* **2008***, 101 (14),* 143902.

15. Maier, S. A.*, Plasmonics: Fundamentals and Applications: Fundamentals and Applications.* Springer: 2007.

16. Earl, S. K.; Gómez, D.; James, T. D.; Davis, T. J.; Roberts, A., Material effects on V-nanoantenna performance. *Nanoscale* **2015***, 7 (9),* 4179-4186.

17. Morin, F., Oxides which show a metal-to-insulator transition at the Neel temperature. *Phys. Rev. Lett* **1959***, 3 (1),* 34-36.

18. Verleur, H. W.; Barker Jr, A.; Berglund, C., Optical Properties of VO_2 between 0.25 and 5 eV. *Phys. Rev.* **1968***, 172 (3),* 788.

19. Goodenough, J. B., The two components of the crystallographic transition in VO_2. J. *Solid State Chem.* **1971,** *3(4),* 490-500.

20. Andreev, V. N.; Klimov, V. A., Effect of deformation on the metal-semiconductor phase transition in vanadium dioxide thin films. *Phys. Solid State* **2011***, 53(3),* 577-582.

21. Zhao, Y.; Hao, J.; Chen, C.; Fan, Z., Electrically controlled metal-insulator transition process in VO_2 thin films. *J. Phys. Condens. Matter* **2012***, 24 (3),* 35601.

22. Jeehoon, K.; Changhyun, K.; Alex, F.; Shriram, R.; Jennifer, E. H., Nanoscale imaging and control of resistance switching in VO_2 at room temperature. *Appl. Phys. Lett.* **2010***, 96,* 213106.

23. Cavalleri, A.; Tóth, C.; Siders, C.; Squier, J.; Ráksi, F.; Forget, P.; Kieffer, J., Femtosecond Structural Dynamics in VO_2 during an Ultrafast Solid-Solid Phase Transition. *Phys. Rev. Lett.* **2001***, 87 (23),* 237401.

24. Cavalleri, A.; Dekorsy, T.; Chong, H.; Kieffer, J.; Schoenlein, R., Evidence for a structurally-driven insulator-to-metal transition in VO_2 : A view from the ultrafast timescale. *Phys. Rev. B* **2004***, 70(16),* 161102.

25. Lysenko, S.; Rúa, A.; Vikhnin, V.; Fernández, F.; Liu, H., Insulator-to-metal phase transition and recovery processes in VO2 thin films after femtosecond laser excitation. *Phys. Rev. B* **2007***, 76 (3),* 35104.

26. Wall, S.; Foglia, L.; Wegkamp, D.; Appavoo, K.; Nag, J.; Haglund, R. F.; Stähler, J.; Wolf, M., Tracking the evolution of electronic and structural properties of VO2 during the ultrafast photoinduced insulator-metal transition. *Phys. Rev. B* **2013**, *87(11)* 115126.

27. Morrison, V. R.; Chatelain, R. P.; Tiwari, K. L.; Hendaoui, A.; Bruhacs, A.; Chaker, M.; Siwick, B. J., A photoinduced metal-like phase of monoclinic VO_2 revealed by ultrafast electron diffraction. *Science* **2014**, *346 (6208),* 445-448.

28. Wegkamp, D.; Herzog, M.; Xian, L.; Gatti, M.; Cudazzo, P.; McGahan, C. L.; Marvel, R. E.; Haglund, R. F.; Rubio, A.; Wolf, M., Instantaneous band gap collapse in photoexcited monoclinic VO_2 due to photocarrier doping. *Phys. Rev. Lett.* **2014**, *113 (21),* 216401.

29. Qazilbash, M.; Brehm, M.; Chae, B.-G.; Ho, P. C.; Andreev, G.; Kim, B.-J.; Yun, S.; Balatsky, A.; Maple, M.; Keilmann, F.; Kim, H.-T.; Basov, D., Mott transition in VO_2 revealed by infrared spectroscopy and nano-imaging. *Science* **2007**, 318 (5857), 1750-1753.

30. Rozen, J.; Lopez, R.; Haglund, R. F.; Feldman, L. C., Two-dimensional current percolation in nanocrystalline vanadium dioxide films. *Appl. Phys. Lett.* **2006**, *88 (8)*, 81902-81902.

31. Chang, Y. J.; Koo, C. H.; Yang, J. S.; Kim, Y. S.; Kim, D. H.; Lee, J. S.; Noh, T. W.; Hyun-Tak, K.; Chae, B. G., Phase coexistence in the metal–insulator transition of a VO2 thin film. *Thin Solid Films* **2005***, 486(1),* 46-49.

32. Joushaghani, A., Kruger, B.A., Paradis, S., Alain, D., Aitchison, J.S., Poon, J.K.S., Sub-volt broadband hybrid plasmonic-vanadium dioxide switches. *Appl. Phys. Lett*. **2013,** 102(6), 061101.

33. Joushaghani, A., Jeong, J., Paradis, S., Alain, D., Aitchison, J.S., Poon, J.K.S., Voltage-controlled switching and thermal effects in VO2 nano-gap junctions. *Appl. Phys. Lett*. **2014,** 104(22), 221904.

34. Cueff, S., Li, D., Zhou, Y., Wong, F.J., Kurvits, J.A., Ramanathan, S., Zia, R., Dynamic control of light emission faster than the lifetime limit using VO2 phase-change. *Nat. Commun*. **2015,** 6.

35. COMSOL www.comsol.com.

36. Palik, E. D., Handbook of Optical Constants of Solids: Index. Academic press: 1998; Vol. 3.

37. Earl, S. K.; James, T. D.; Marvel, R. E.; Gomez, D. E.; Davis, T. J.; Valentine, J. G.; McCallum, J. C.; Haglund, R. F.; Roberts, A., Vanadium dioxide thickness effects on tunable optical antennas. *SPIE Micro+ Nano Materials, Devices, and Applications* **2013**, pp. 89232S-89232S.

38. Marvel, R.; Appavoo, K.; Choi, B.; Nag, J.; Haglund Jr, R. F., Electron-beam deposition of vanadium dioxide thin films. *Appl. Phys. A* **2013***, 111 (3),* 975-981.

39. Kana, J. B. K.; Ndjaka, J. M.; Vignaud, G.; Gibaud, A.; Maaza, M., Thermally tunable optical constants of vanadium dioxide thin films measured by spectroscopic ellipsometry. *Opt. Commun.* ***2011****, 284(3),* 807-812.

40. Cadusch, J. J.; James, T. D.; Roberts, A., Experimental demonstration of a wave plate utilizing localized plasmonic resonances in nanoapertures. *Opt. express* ***2013****, 21 (23),* 28450-28455.

41. Collett, E., Measurement of the four Stokes polarization parameters with a single circular polarizer. *Opt. Commun.* ***1984****, 52 (2), 77-80.*

42. thorlabs https://www.thorlabs.com.

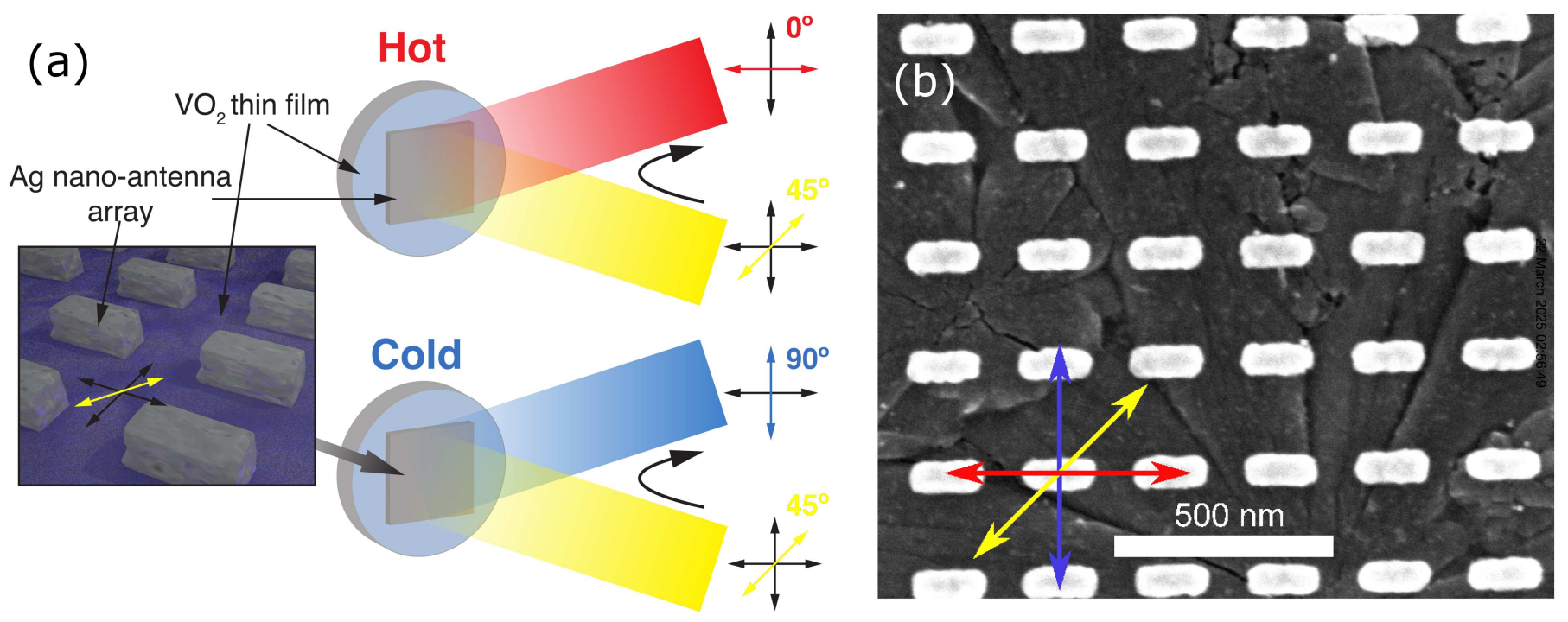
(a)
Hot
VO_2 thin film
Ag nano-antenna array
0°
45°
Cold
90°
45°
(b)
500 nm
22 March 2025 02:56:49

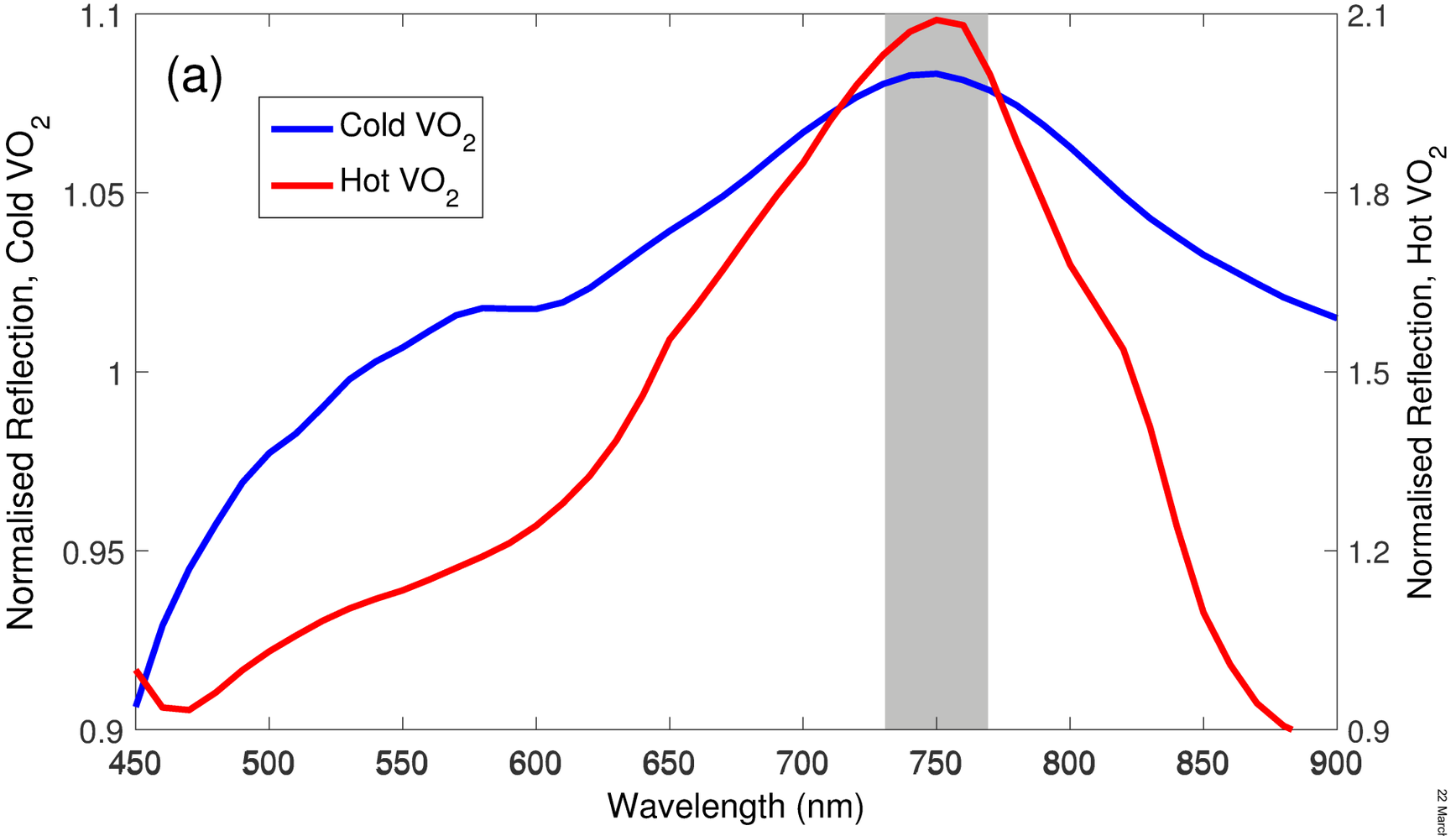

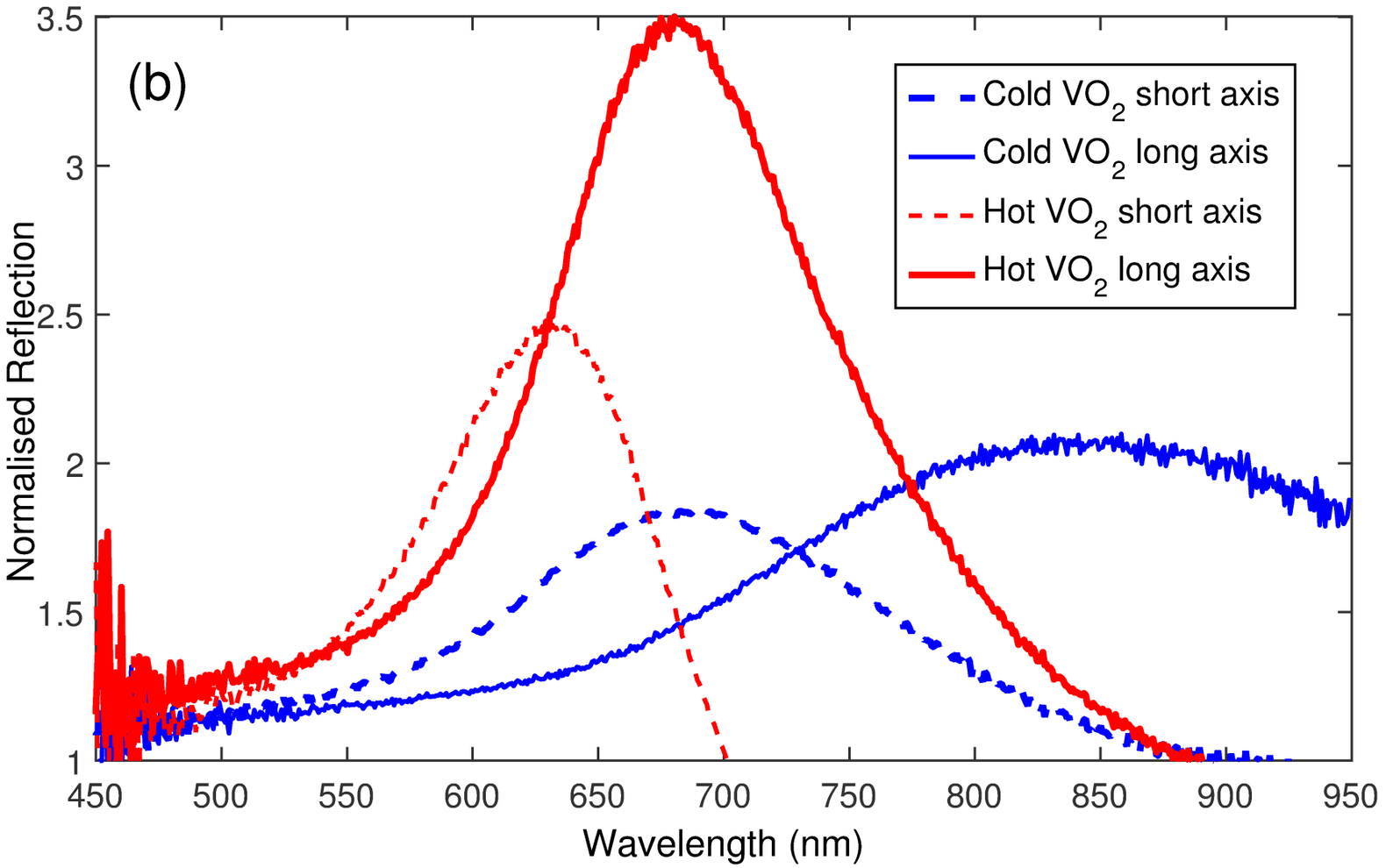

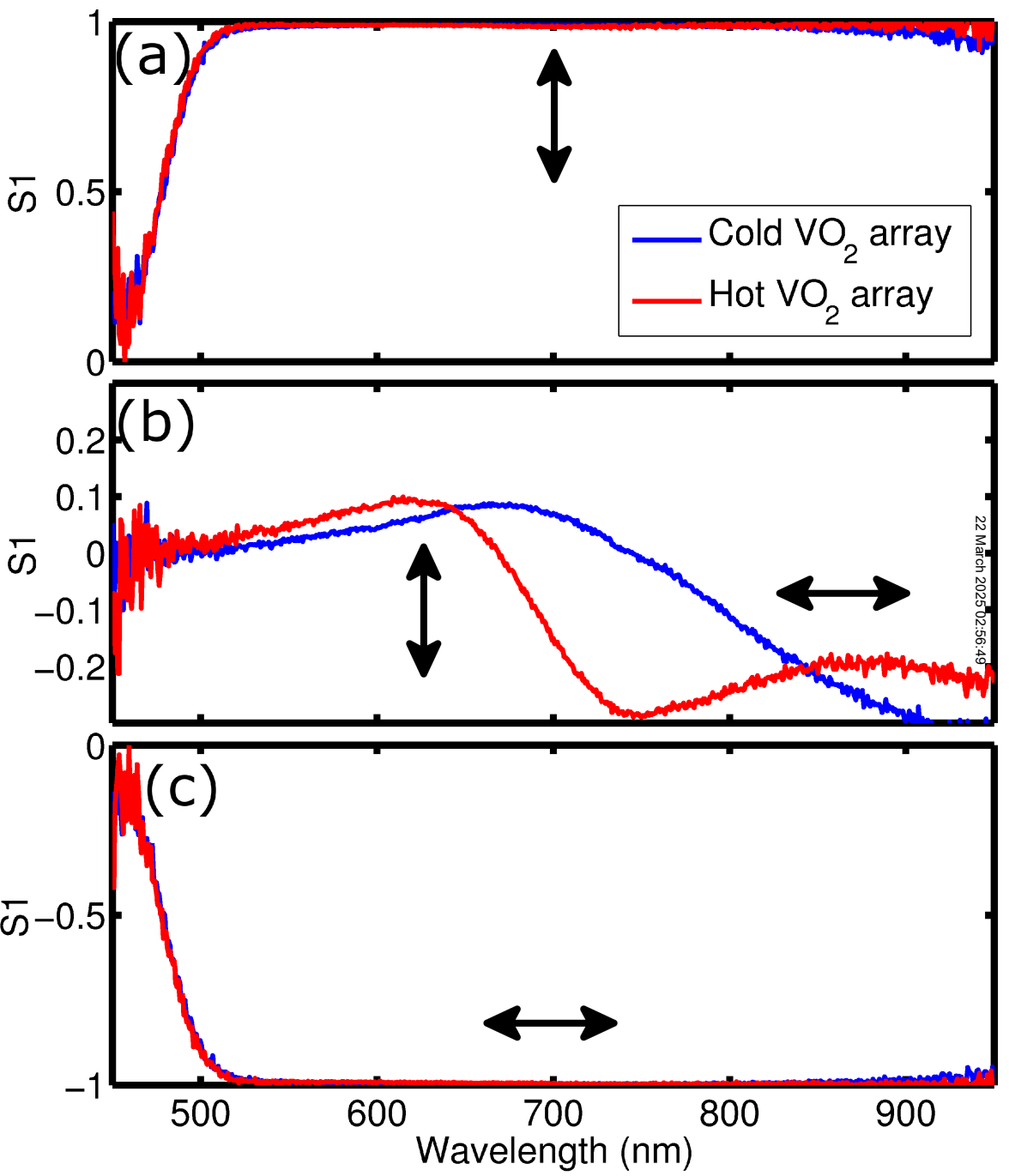
(a)
(b)
(c)
S1
1
0.5
0
0.2
0.1
−0.1
−0.2
−0.5
−1
Cold VO2 array
Hot VO2 array
500
600
700
800
900
Wavelength (nm)
22 March 2025 02:56:49